Immunodeficient Mouse Strains Display Marked Variability in Growth of Human Melanoma Lung Metastases

Beatriz M. Carreno,[1] Joel R. Garbow,[5,6] Grant R. Kolar,[3] Erin N. Jackson,[4] John A. Engelbach,[5] Michelle Becker-Hapak,[1] Leonidas N. Carayannopoulos,[1] David Piwnica-Worms,[2,4,6] and Gerald P. Linette[1]

Abstract

Purpose: Immunodeficient mice serve as critical hosts for transplantation of xenogeneic cells for *in vivo* analysis of various biological processes. Because investigators typically select one or two immunodeficient mouse strains as recipients, no comprehensive study has been published documenting differences in human tumor engraftment. Taking advantage of the increased metastatic potential of RhoC-expressing human (A375) melanoma cells, we evaluate four immunodeficient mouse strains: severe combined immunodeficiency (*scid*), nonobese diabetic (NOD)-*scid*, NOD-*scid* $\beta 2m^{null}$, and NOD-*scid IL2R*γ^{null} as xenograft tumor recipients.

Experimental Design: Bioluminescence, magnetic resonance imaging, and histopathology were used to monitor serial tumor growth. Natural killer (NK) cell function was examined in each mouse strain using standard ^{51}Chromium release assays.

Results: Melanoma metastases growth is delayed and variable in *scid* and NOD-*scid* mice. In contrast, NOD-*scid* $\beta 2m^{null}$ and NOD-*scid IL2R*γ^{null} mice show rapid tumor engraftment, although tumor growth is variable in NOD-*scid* $\beta 2m^{null}$ mice. NK cells were detected in all strains except NOD-*scid IL2R*γ^{null}, and *in vitro* activated *scid*, NOD-*scid*, and NOD-*scid* $\beta 2m^{null}$ NK cells kill human melanoma lines and primary melanoma cells. Expression of human NKG2D ligands MHC class I chain–related A and B molecules renders melanoma susceptible to murine NK cell–mediated cytotoxicity and killing is inhibited by antibody blockade of murine NKG2D.

Conclusions: Murine NKG2D recognition of MICA/B is an important receptor-ligand interaction used by NK cells in immunodeficient strains to limit engraftment of human tumors. The absolute NK deficiency in NOD-*scid IL2R*γ^{null} animals makes this strain an excellent recipient of melanoma and potentially other human malignancies.

Mouse models of human cancer serve as essential experimental systems, and genetically defined immunodeficient mouse strains constitute a valuable tool for studying tumorigenesis. Athymic (nude) mice have been the standard for establishing *in vivo* models of human malignancies (1). However, the presence of residual adaptive and innate immunity can interfere with the establishment of tumor xenografts. Athymic mice develop small numbers of mature αβTCR lymphocytes with age; in addition, robust natural killer (NK) cell activity is present and increases with age (2, 3). Numerous reports confirm variable rates of human tumor growth in athymic animals (4–6); for example, of 200 human breast cancer samples tested in nude mice, just 25 (12.5%) grew as xenografts at the site of s.c. implantation (7). Severe combined immunodeficiency (scid) mice have relative B- and T-cell deficiencies and are often used as recipients of human xenografts. Improved tumor engraftment rates have been reported in the nonobese diabetic (NOD)-*scid* strain, where introduction of the scid mutation into the NOD background results in reduced macrophage and NK function, as well as an absence of complement-dependent hemolytic activity (8, 9). Recently, two additional immunodeficient strains have been described as follows: NOD-*scid* $\beta 2m^{null}$ and NOD-*scid IL2R*γ^{null} (10). The NOD-*scid* $\beta 2m^{null}$ strain was developed by backcrossing the $\beta 2m^{null}$ mutation to the NOD-*scid* strain resulting in mice deficient in MHC class I expression (NOD-*scid* $\beta 2m^{null}$). Accumulating data suggest that NK cells that develop in a MHC class I–deficient background are unlicensed and, hence, unable to kill susceptible targets

Authors' Affiliations: Departments of [1]Medicine, [2]Developmental Biology, [3]Pathology-Immunology, [4]Molecular Imaging Center, and [5]Biomedical Magnetic Resonance Laboratory, Mallinckrodt Institute of Radiology, and [6]Siteman Cancer Center, Washington University School of Medicine, St Louis, Missouri

Received 9/27/08; revised 1/14/09; accepted 2/11/09; published online 5/15/09.

Grant support: ACS IRG-58-010-49 (G. Linette), NIH P50 CA94056 (D.P. Worms), NIH/National Cancer Institute R24 CA 83060 and National Cancer Institute P30 CA91842 (J. Garbow), and NIH/NIAID K08 AI57361 (L.N. Carayannopoulos).

The costs of publication of this article were defrayed in part by the payment of page charges. This article must therefore be hereby marked *advertisement* in accordance with 18 U.S.C. Section 1734 solely to indicate this fact.

Requests for reprints: Beatriz M. Carreno, Washington University School of Medicine, Division of Oncology, 660 South Euclid Avenue, Campus Box 8007, St Louis, MO 63110. Phone: 314-362-9407; Fax: 314-362-9333; E-mail: bcarreno@wustl.edu.

doi:10.1158/1078-0432.CCR-08-2502

Translational Relevance

Immunodeficient mice are widely used in cancer research to study human cancer biology and evaluate new therapeutics. Although the athymic nude mouse has served as the standard recipient for over 40 years, new immunodeficient mouse strains have been developed that possess well-defined defects in adaptive and innate immunity. In this article, we examined the influence of residual innate immunity on the development of pulmonary metastases using the human A375-RhoC melanoma. The integration of small animal imaging with a clinically relevant lung metastases model reveals the inherent variability among the Severe combined immunodeficiency (*scid*), nonobese diabetic (NOD)-*scid*, and NOD-*scid* β_2m ^{null} strains. Genetic ablation of the IL2Rγ chain leads to an absolute natural killer deficiency in the NOD-scid IL2Rγ^{null} strain and results in consistent engraftment of human melanoma. Our observation expands the potential to study human melanoma and establishes a new standard to evaluate novel agents in a clinically relevant animal model.

upon activation (11). The NOD-*scid IL2R*γ ^{null} strain was developed by introduction of the *IL2R*γ^{null} mutation into the NOD-*scid* strain (12). Absence of *IL2R*γ, the common cytokine-receptor γ-chain shared by the interleukin (IL)-2, IL-4, IL-7, IL-9, IL-15, and IL-21 receptors leads to impaired NK cell development due to absence of IL-15 signaling (13). Improved engraftment of human cord blood CD34+ cells has been reported in NOD-*scid* *β2m*^{null} and NOD-*scid IL2R*γ^{null} highlighting the potential use of these strains as recipients of tumor xenografts (14).

Animal models of human melanoma are limited. Clark et al. (15) generated highly metastatic human melanoma (A375) cells through *in vivo* selection of lung metastasis in nude mice. A genomic analysis of metastatic A375 variants showed that RhoC, an RAS-related guanosine triphosphatase, is an important determinant of tumor cell invasion. Further studies have shown that RhoC plays a role in cytoskeleton organization and is essential for tumor metastasis (16). In a recent series of studies, Beige-*scid* mice were used to evaluate therapeutics for human melanoma A375-RhoC pulmonary metastasis (17, 18). However, NK cell function was not studied and because no other mouse strains were evaluated, the relative effect of residual innate immunity remains undefined in the A375-RhoC model.

In the present study, we evaluate human melanoma (A375-RhoC) pulmonary metastases in four immunodeficient mouse strains: *scid*, NOD-*scid*, NOD-*scid* *β2m*^{null}, and NOD-*scid IL2R*γ^{null} strains. Tumor growth was monitored noninvasively by imaging using bioluminescence (BLI) and magnetic resonance imaging (MRI) combined with histopathologic assessment. BLI allowed for accurate, real-time serial *in vivo* quantitation of tumor burden, whereas MRI permitted three-dimensional structural imaging of tumor. Our results show that NOD-*scid IL2R*γ^{null} mice are highly permissive for engraftment of human melanoma metastases, whereas endogenous NK activity in the other three strains delayed or, in certain instances, completely prevented the formation of pulmonary metastasis. Importantly, we show that expression of human NKG2D ligands MHC class I chain–related A (MICA) and B (MICB) molecules by melanoma confers susceptibility to murine NK-mediated cytotoxicity.

Materials and Methods

Mouse strains. CB17-*Prkdc*^{scid}/J (*scid*), NOD.CB17-*Prkdc*^{scid}/J (NOD-*scid*), NOD.Cg-*Prkdc*^{scid} *B2m*^{tm1Unc}/J (NOD-*scid* *β2m*^{null}), and NOD.Cg-*Prkdc*^{scid} *IL2r*γ^{tm1Wjll}/SzJ (NOD-*scid IL2R*γ^{null}) mice were obtained from The Jackson Laboratory and bred and housed according to the guidelines of Washington University, Division of Comparative Medicine. Strain background is BALB/c (H-2^{d}) for *scid* and NOD (H-2^{g7}) for all other strains. The animal ethics committee approved all experiments. All mice used were between ages 7 and 14 wk.

Melanoma cell lines. The human melanoma cell line A375P-RhoC-*GFP* (15) was transduced with a retrovirus expressing a click beetle red luciferase (*cbr-luc*)/enhanced yellow fluorescence protein (e*YFP*) fusion gene. A stable cell line was selected by flow cytometry on a MoFlo sorting for cells expressing high *GFP* (for RhoC expression) and e*YFG* (for *cbr-luc* expression) levels. Stable A375 RhoC-luciferase–expressing cell line is called A375RC-Luc. Human melanoma lines DM6 and Lox (American Type Culture Collection) are previously described (19). CG mel is a primary human melanoma (S100+ HMB45+) generated in our laboratory from a resected lymph node metastases. DM6, Lox, and CG lines stably expressing high *GFP* (for RhoC expression) and e*YFG* (for

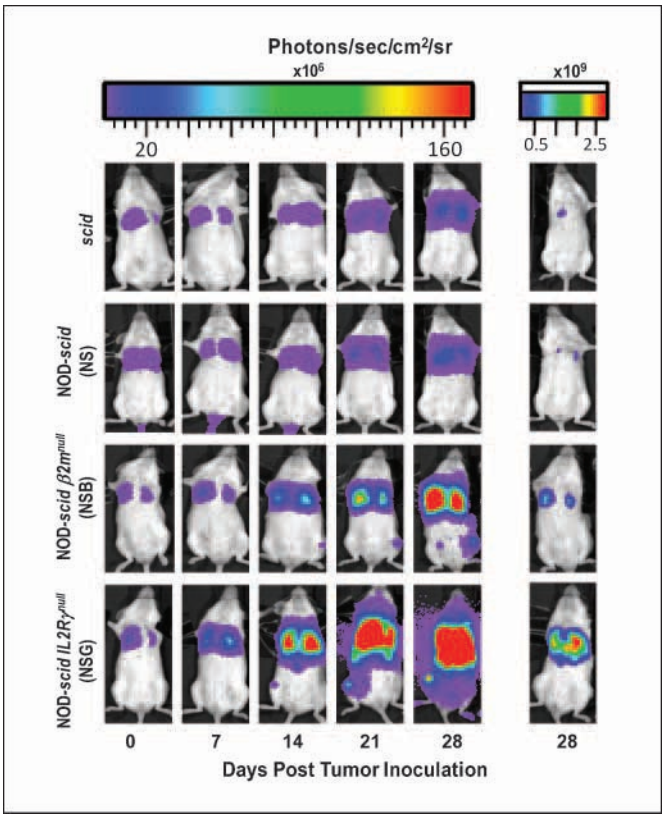

Fig. 1. Human melanoma (A375RC-luc) engraftment in *scid*, NOD-*scid* (*NS*), NOD-*scid* *β2m*^{null} (*NSB*), and NOD-*scid IL2R*γ^{null} (*NSG*) mice. Melanoma tumor growth was monitored by weekly BLI. 2.5 × 10^6 A375 melanoma cells expressing RhoC/luciferase (A375RC-luc) were injected i.v., and mice were imaged 2 to 3 h after injection (day 0) and weekly thereafter. Weekly images from a representative mouse per strain formatted on an identical scale are shown. Reformatted images from day 28 are shown on a separate scale to show tumor confinement (bioluminescence signal) to the lungs.

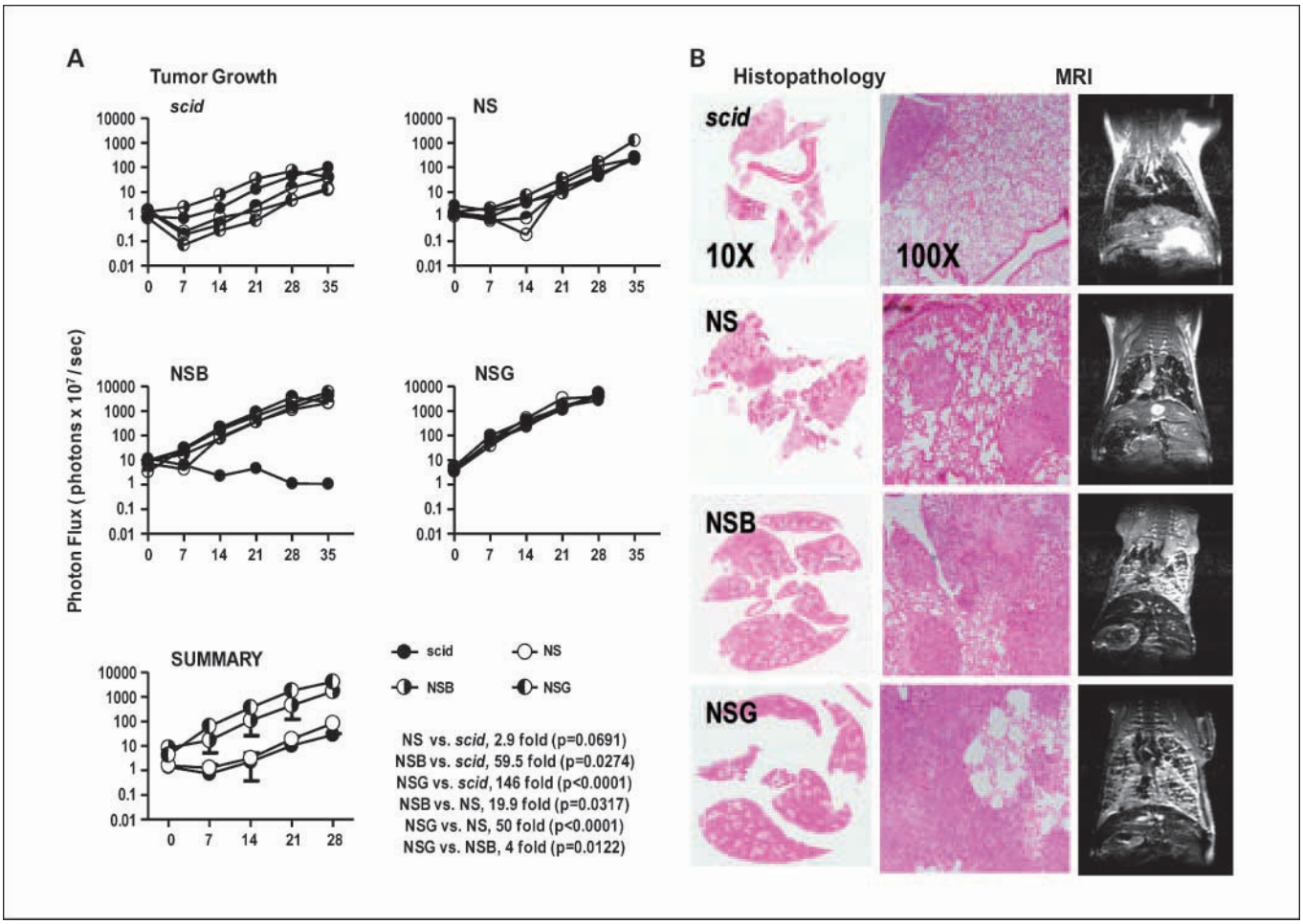

Fig. 2. Tumor growth, histopathology and MRI of melanoma pulmonary metastasis in immunodeficient mouse strains. *A*, tumor growth was measured as photon flux (photons × 10^7/s) at indicated times after A375RC-luc injection. A representative experiment is shown with five mice per group (data shown in log scale). Note that one mouse in the NOD-*scid* $\beta2m^{null}$, group rejected the A375 melanoma. A summary of tumor growth (±SD) among strains is shown in *SUMMARY*. On day 28, pair-wise differences in bioluminescent photon counts were statistically analyzed by the unpaired *t* test. Fold mean increases between strains are indicated with respective *P* values. *B*, histopathology and MRI of melanoma pulmonary metastasis in immunodeficient strains. At day 28 (NOD-*scid IL2R*γ^{null}) or day 35 (all other strains) tumor growth was monitored by MRI imaging. Representative slides at ×10 and ×100 magnifications are shown. Mean tumor burden is estimated as percentage of total lung parenchyma; tumor burden in each strain (average of 2 mice) is as follows: *scid*, 7%; NOD-*scid*, 35%; NOD-*scid* $\beta2m^{null}$, 62%; and NOD-*scid IL2R*γ^{null}, 95%. One representative MRI coronal image per mouse per strain is shown.

cbr-luc expression) levels were generated as described above for A375. M14 melanoma cells (20) were transfected with MICA and MICB cDNA (21) using lipofectamine as directed by manufacturer's instructions (Invitrogen). Clones were selected using G418 at 1 mg/mL and stable expression of MICA and MICB confirmed by flow cytometry using anti-MICA/B monoclonal antibody (mAb) 6D4 (Biolegend; ref. 22). Expression of ULBP1-3 by melanoma cell lines was determined by flow cytometry using antibodies (23) obtained from Axxora.

In vivo *imaging*. For serial analysis of tumor growth, mice were injected i.v. with 2.5 × 10^6 RhoC/luciferase-expressing tumor cells in 200 μL PBS. After tumor inoculation (2-3 h), mice were injected i.p. with 150 mg/kg D-luciferin (Biosynth)/PBS and imaged 10 min later. Imaging was done using a charge-coupled device camera (IVIS 50; Caliper Corporation; exposure time, 1-30 s; binning, 8; field of view, 12; f/stop 1, open filter) at the Molecular Imaging Center (Washington University, St. Louis) as described previously (24). Mice were anesthetized using isoflourane (2.5% vaporized in O_2). For analysis, total photon flux (photons per second) was measured from a fixed region of interest over the thorax/liver area using Living Image 2.50 and IgorPro software (Wavemetrics; ref. 24). Animals were monitored biweekly for health and signs of tachypnea and weight loss. MRI experiments were done in the Biomedical MR Laboratory (Washington University, St. Louis) as previously described (25, 26). Briefly, respiratory gated, spin-echo MR images were collected in a 4.7 T Oxford magnet interfaced with a Varian NMR Systems INOVA console. Animals were anesthetized with isoflourane (1% v/v in O_2) and animal core body temperature was maintained at 37°C ± 1°C by circulation of warm air through the bore of the magnet. Synchronization of MR data collection with animal respiration was achieved with a home-built respiratory-gating unit (27) and all images were collected during postexpiratory periods. Imaging parameters were as follows: TR, 3 s; TE, 20 ms; field of view, 2.5 cm; slice thickness, 0.5 mm. BLI was done weekly; MRI experiments were done at selected time points as described.

Histopathology. After MRI on day 28 (for NOD-*scid IL2R*γ^{null}) or day 35 (all other strains), animals were sacrificed, lungs were excised, and fixed in 10% formalin overnight. Paraffin-embedded tissues were sectioned and stained by H&E. Tissues were examined in a blinded manner; at least five sections of tumor were examined by a pathologist. Two animals per strain were evaluated. Representative slides from each animal were scanned with modified 35-mm slide scanner, areas of tumor were quantified and expressed as a percentage of total lung tissue using NIH Image Software (NIH).

Immunologic assays. Spleen cell suspensions were prepared and stained using anti-CD3, anti-CD45.1, anti-CD49b-PE (DX5), and/or

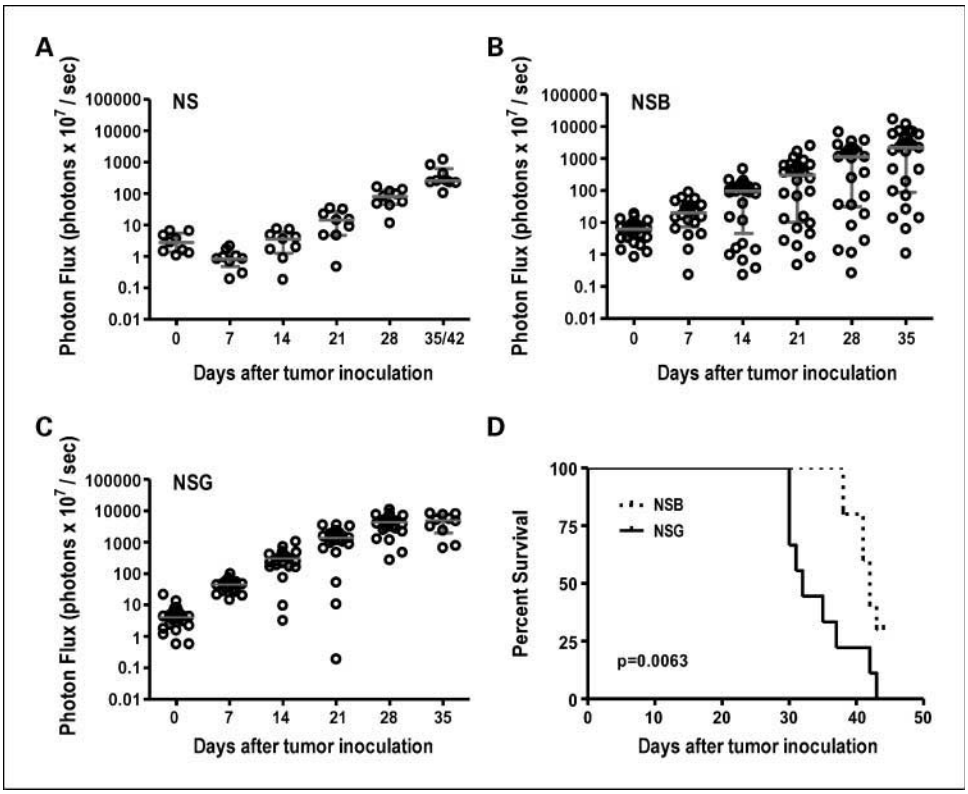

Fig. 3. Tumor growth and survival in NOD-*scid*, NOD-*scid* $\beta 2m^{null}$, and NOD-*scid IL2R*γ^{null} mice. Tumor growth was monitored by BLI: (*A*) NOD-*scid* ($n = 14$), (*B*) NOD-*scid* $\beta 2m^{null}$ ($n = 28$), and (*C*) NOD-*scid IL2R*γ^{null} ($n = 32$). Summary scatter dot plots with each dot representing one mouse are shown. Data represents four independent experiments. *Horizontal line,* median value; *top and bottom of the whiskers plot,* 75% and 25% percentile, respectively. *D,* survival curve of tumor-bearing NOD-*scid* $\beta 2m^{null}$ and NOD-*scid IL2R*γ^{null} mice. Mice were injected i.v. with 2.5×10^6 A375RC-luc cells and monitored weekly by BLI ($n = 10$ mice per strain). Mice were sacrificed if weight dropped below 20% of initial. Curves were compared using the log-rank test. One of three independent experiments is shown.

anti–NKG2D-biotin (28). Antibodies were obtained from eBioscience or Biolegend. Cells were incubated with anti-CD32/CD16 for 5 min at 4°C, followed by specific antibodies, washed, and, in the case of anti-NKG2D biotin, followed by SA-APC. Staining with murine (mu) NKG2D and control tetramer was done as described (29). Multiparameter flow cytometry analysis was done using a BD Biosciences FACScan flow cytometer modified with a second, 633 nm 25 mW laser, and 2 additional detectors with bandwidths at 660 and 760 nm. For assessment of NK function, spleen cell suspensions were depleted of RBC and cultured at 2×10^6 cells/mL in 24-well tissue culture plates for 48 h in RPMI/10% FCS/2 mmol/L glutamine, HEPES, Pen-Strep, murine IL-15 (100 ng/mL; Peprotec) and murine IL-18 (100 ng/mL; R&D Systems). For ^{51}Cr-release assays, target cells (10^6 cells/mL) were labeled with 1 μmol/L ^{51}Cr for 1 h, washed and added to spleen cultures at various effector/target (E/T) ratios, and incubated in triplicate for an additional 4 h. ^{51}Cr-release was quantitated in a Tri-Lux Wallac as described (30).

Statistical analysis. Unpaired *t* test was done to evaluate tumor growth kinetics among strains, and the differences were significant if *P* value was <0.05. The Interquartile range were determined to evaluate tumor growth variability among strains, and Kaplan-Meier product-limit method was used to calculate survival rates; differences between groups were determined using log-rank analysis; *P* values of <0.05 indicate significance in survival rates. Repeated measure one-way ANOVA was done to evaluate lysis of melanoma by NK cells; for pairwise comparison, a Tukey's test was done post-ANOVA analysis. All analysis was done using Prism version 5 (GraphPad Software, Inc.).

Results

Human melanoma pulmonary metastases show different rates of engraftment in immunodeficient mouse strains. Human melanoma cells expressing RhoC (A375-RhoC) exhibit lung tropism after i.v. transplantation in athymic mice (15). To evaluate the effect of residual murine innate immunity on the development of human melanoma pulmonary metastases, we assessed A375-RhoC growth in *scid*, NOD-*scid*, NOD-*scid* $\beta 2m^{null}$, and NOD-*scid IL2R*γ^{null}. BLI and MRI imaging modalities were used to monitor rates of tumor engraftment (25, 31). A375-RhoC cells stably expressing a luciferase reporter (A375RC-Luc, 2.5×10^6) were administered i.v. on day 0 and animals were examined using BLI 2 to 3 hours after tumor inoculation and weekly thereafter to assess the kinetics of tumor growth (31). Serial BLI images of one representative mouse per strain are shown in Fig. 1. Tumor growth as assessed by BLI signal intensity is most rapid in NOD-*scid IL2R*γ^{null} animals followed by the NOD-*scid* $\beta 2m^{null}$ strain (Fig. 2A). The growth of melanoma lung metastasis was delayed in *scid* and NOD-*scid* mice when compared with NOD-*scid IL2R*γ^{null} and NOD-*scid* $\beta 2m^{null}$ (Fig. 2A). The mean time to reach a photon flux of 1×10^9 photon/second was as follows: *scid*, 31d; NOD-*scid*, 28d; NOD-*scid* $\beta 2m^{null}$, 14d; and NOD-*scid IL2R*γ^{null}, 8d (Fig. 2A). As tissue attenuation of BLI signal is fixed at any given depth, different times to reach equivalent BLI signals are likely to reflect distinct tumor growth kinetics among strains. Tumor growth was confined to the lung in all strains as no BLI signal was detected outside this organ (Fig. 1). Imaging results were verified by necropsy on day 28 to 35 (data not shown).

To further characterize tumor growth and correlate BLI with anatomy, MRI was done on two animals per strain. Coronal, respiratory-gated spin-echo images of a representative mouse per strain (day 28 for NOD-*scid IL2R*γ^{null}; day 35 all other strains) are shown together with histopathology of lung tissue (H&E-stained sections; Fig. 2B). Two views, ×10 and ×100, of lung tissue sections are shown for comparison.

Based on total lung parenchyma, quantitative tumor burden for each strain (n = 2 mice per strain) was assessed microscopically in a blinded manner: *scid*, 7%; NOD-*scid*, 35%; NOD-*scid* $\beta 2m^{null}$, 62%; and NOD-*scid IL2R*γ^{null}, 95%. MRI detection of pulmonary metastases is less sensitive than BLI; in *scid* mice, BLI shows clear signal on day 35, although no solid tumor is detected by MRI. In contrast, innumerable pulmonary metastases are visualized in both NOD-*scid* $\beta 2m^{null}$ and NOD-*scid IL2R*γ^{null} strains (Fig. 2B, *right column*). Although several lung nodules are evident in the NOD-*scid* animals, the tumor burden is substantially less and is consistent with the BLI results.

Human melanoma shows variable engraftment in NOD-scid β2m^{null}. We did additional experiments to further characterize the kinetics of tumor growth in the three most permissive strains: NOD-*scid*, NOD-*scid* $\beta 2m^{null}$, and NOD-*scid IL2R*γ^{null}. Figure 3A to C shows a summary of tumor growth rates as determined by BLI for individual animals at weekly time points. BLI signal is reproducibly detected in all animals within 2 to 3 hours after i.v. injection of A375RC-luc cells. In spite of brisk tumor growth in both NOD-*scid* $\beta 2m^{null}$ and NOD-*scid IL2*γ^{null}, tumor engraftment is highly variable in NOD-*scid* $\beta 2m^{null}$ as shown by the larger interquartile range among mice in the NOD-*scid* $\beta 2m^{null}$ strain (Fig. 3B). Between day 28 and 35, 60% of NOD-*scid IL2R*γ^{null} mice died due to tumor progression. In contrast, no deaths were seen before day 35 in any tumor-bearing NOD-*scid* and NOD-*scid* $\beta 2m^{null}$ animal; NOD-*scid* mice show significantly delayed tumor growth compared with NOD-*scid* $\beta 2m^{null}$ and NOD-*scid IL2R*γ^{null} mice. Survival curves of NOD-*scid* $\beta 2m^{null}$ and NOD-*scid IL2R*γ^{null} in a representative experiment (n = 10 mice per cohort) are shown in Fig. 3D. The median survival was 42 days for NOD-*scid* $\beta 2m^{null}$ and 32 days for NOD-*scid IL2R*γ^{null}; in contrast, all NOD-*scid* mice survived past 48 days (data not shown).

Rapid engraftment of multiple human melanoma lines in NOD-scid IL2Rγ^{null} mice. Due to the consistent and reproducible growth of A375RC-luc observed in NOD-*scid IL2R*γ^{null}, we selected this mouse strain to evaluate the growth of three additional Rho-C/luciferase expressing human melanoma cell lines. DM6 (19) and Lox are well-characterized cell lines, whereas CG mel is a primary (low passage) melanoma line isolated in our laboratory. NOD-*scid* mice (strain background NOD: H-2^{g7}) were used as the comparator strain with NOD-*scid IL2R*γ^{null} mice as these strains share identical genetic background (10). Average BLI values for mice (n = 3) at each time point is shown in Fig. 4A to D. Each melanoma studied exhibited a distinct rate and level of engraftment in NOD-*scid* and NOD-*scid IL2R*γ^{null} mice as assessed by BLI. Rates and levels of engraftment of A375, Lox, and CG were higher in NOD-*scid IL2R*γ^{null} relative to NOD-*scid* mice. Interestingly, despite similar BLI signal at day 0 in DM6-bearing NOD-*scid* and NOD-*scid IL2R*γ^{null}, no BLI signal was detected after day 7 in NOD-*scid* mice, suggesting complete rejection of DM6 in this strain. In agreement with this finding, no evidence of tumor was observed upon autopsy of DM6-bearing NOD-*scid* lungs (day 50 after tumor inoculation; data not shown). Altogether, these results show that NOD-*scid IL2R*γ^{null} mice are a permissive host for engraftment of human melanoma pulmonary metastasis.

NK characterization and function in immunodeficient strains. The superior engraftment of human melanoma in NOD-*scid IL2R*γ^{null}, a strain devoid of NK cells, implicated murine NK cells as the effector population responsible for tumor rejection. Flow cytometry analysis confirms the presence of NK cells in *scid* (48.9%), NOD-*scid* (27.3%), and NOD-*scid* $\beta 2m^{null}$

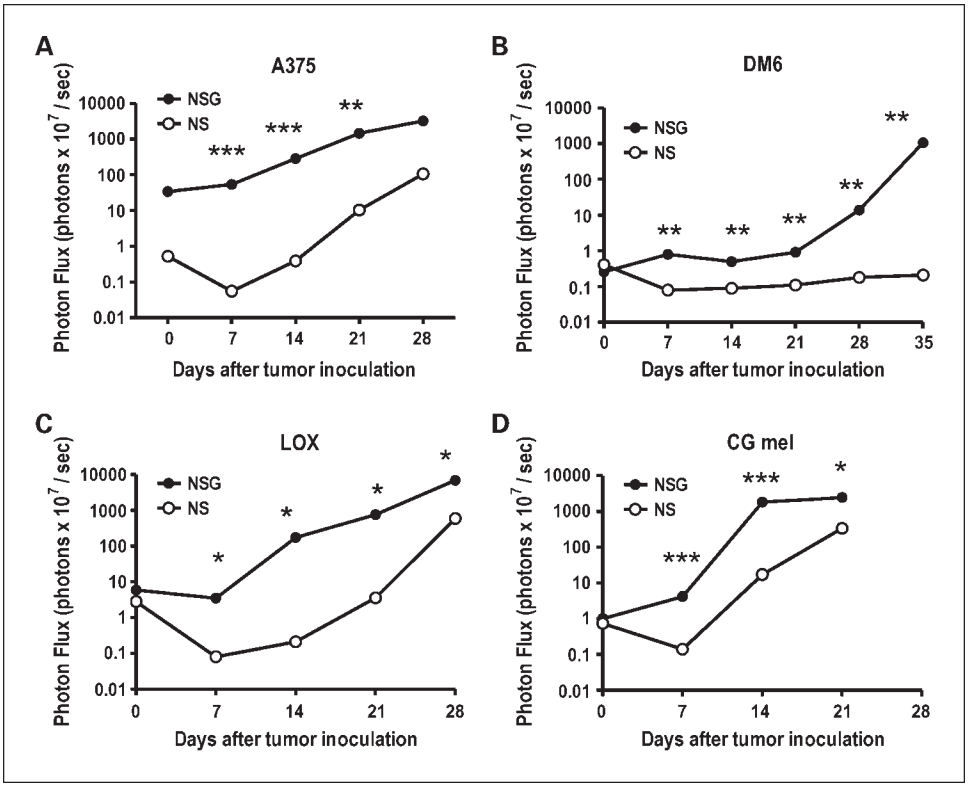

Fig. 4. NOD-*scid IL2R*γ^{null} mice are permissive for growth of multiple melanoma lines. NOD-*scid* or NOD-*scid IL2R*γ^{null} were injected i.v. with 2.5 × 10^6 (*A*) A375, (*B*) DM6, (*C*) Lox, or (*D*) CG mel (a primary melanoma cell line) expressing RhoC/luciferase; tumor growth was monitored by weekly bioluminescence. Average photon flux is shown (n = three mice/strain/line). In all instances, melanoma pulmonary metastases grew faster in the NOD-*scid IL2R*γ^{null} mice. Pair-wise differences in bioluminescent photon counts were statistically analyzed by the unpaired t test at each time point, P values are shown as follows: *, $P < 0.05$; **, $P < 0.005$; ***, $P < 0.0005$.

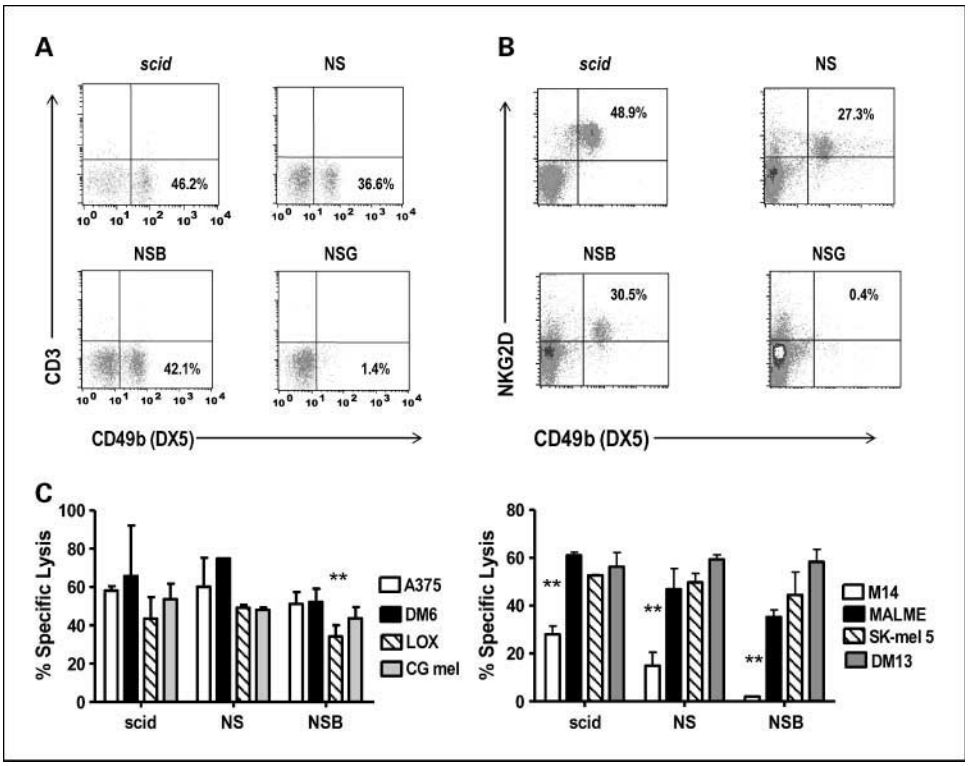

Fig. 5. NK cell populations in *scid*, NOD-*scid*, and NOD-*scid* $\beta 2m^{null}$ mouse strains display *in vitro* cytotoxicity against human melanoma cell lines. Spleen cell suspensions were stained with (*A*) anti-CD45.1; anti-CD3 and anti-pan NK cell (*DX5*) antibodies; or (*B*) anti-CD45.1, anti-pan NK cell (*DX5*), and anti-NKG2D antibodies. Percentages are reported based on CD45.1+ gated cells; within the whole spleen cell population (CD45.1+ and CD45.1–), DX5/NKG2D double positive cells are 12.6%, 8.8%, and 9.3% in *scid*, NOD-*scid*, and NOD-*scid* $\beta 2m^{null}$, respectively. In NOD-*scid IL2R*γ^{null} spleen cells, no reactivity was observed with DX5 antibody and anti-NGK2D mAb confirming the absence of NK cells in NOD-*scid IL2R*γ^{null}. A representative mouse ($n = 5$) is shown. *C*, IL-15 + IL-18–activated NK cells from *scid*, NOD-*scid*, and NOD-*scid* $\beta 2m^{null}$ display cytotoxic activity against human melanoma lines. Spleen cells (2×10^6cells/mL) were activated with IL-15 (100 ng/mL) and IL-18 (100 ng/mL) for 48 h, harvested, and used as effectors in a 4-h ^{51}Cr-release assay. IL-15 + IL-18–treated NOD-*scid IL2R*γ^{null} spleen cells did not yield any viable cells. In the experiment shown, the E/T ratio is 30:1. YAC cells were used as the positive control (data not shown). Data are representative of four independent experiments. Lysis of melanoma cell lines by each mouse strain was analyzed by repeated measure one-way ANOVA followed by Tukey's analysis. **, *P* values of <0.005 are statistically significant.

(30.5%) spleen CD45+ populations as determined by the coexpression of CD49b (DX5) and NKG2D. No reactivity of NOD-*scid IL2R*γ^{null} spleen cells was observed with anti-CD49b or anti-NKG2D, indicating that NK cells were absent in this mouse strain as previously noted (Fig. 5A and B; ref. 13).

To assess NK effector function, spleen cells from the various strains were activated *in vitro* with IL-15 + IL-18 and, 48 hours later, assessed for their capacity to recognize human melanoma cells as targets in a ^{51}Cr-release assay. NOD-*scid IL2R*γ^{null} spleen cells cultured in IL-15 + IL-18 yielded no appreciable numbers of NK cells and displayed no killing against human melanoma or YAC cells, confirming the complete absence of NK cells in this strain (data not shown). IL-15 + IL-18–activated *scid*, NOD-*scid*, and NOD-*scid* $\beta 2m^{null}$ spleen cells were able to recognize and kill YAC cells (data not shown), as well as multiple human melanoma lines (Fig. 5C). These findings indicate that murine NK cells from selected immunodeficient mice have the ability to recognize human melanoma.

Expression of NKG2D ligands MICA, MICB, and UL-16 binding proteins 1 to 3 by human melanoma. MICA and MICB and UL-16 binding proteins (ULBP) 1 to 3 are the human ligands for NKG2D, a NK activating receptor (32). Several reports provide evidence that muNKG2D can bind human NKG2D ligands such as MICB, ULBP-1, and ULBP-2 (33, 34). To further investigate the mechanism of murine NK recognition of human melanoma, we determined the expression of NKG2D ligands on selected melanoma cell lines, including M17 a melanoma cell line obtained from the European Searchable Tumor Cell Line and Data Bank and reported as MICA/B negative (35). As shown in Fig. 6A, ULBP-1, ULBP-2, and ULBP-3 expression among melanoma cell lines was heterogeneous. Most lines were negative for ULBP-1, and expressed variable levels of ULBP-2 and ULBP-3. Only one cell line, DM6, expressed all three ULBP molecules. No correlation was observed between ULBP expression and the ability of murine NK cells to recognize human melanoma. In contrast, seven of nine melanoma cell lines expressed MICA/B as detected by the 6D4 mAb (22). Interestingly, low levels of MICA/B expression in M14 and M17 cells correlated with low susceptibility to murine NK cell cytotoxicity (Figs. 6A-B and 7A), suggesting a potential role for MICA/B in murine NK cytotoxicity against human melanoma cells.

MICA and B expression by human melanoma confers susceptibility to muNKG2D-mediated cytotoxicity. To investigate MICA/B-muNKG2D interactions and its functional consequences, M14 cells were transfected with MICA or MICB and evaluated for binding of muNKG2D tetramer (29). As shown in Fig. 6B, M14 cells show no reactivity with MICA/B mAb and exhibit low levels of muNKG2D tetramer binding. This finding is consistent with low level expression of ULBP-2 by M14 because muNKG2D

tetramer can bind ULBP-2 as shown by Sutherland et al. (34). M14 cells were transfected with cDNA encoding MICA or MICB and expression was confirmed using the 6D4 mAb. Moreover, expression of MICA and MICB in M14 cells results in increased binding of muNKG2D tetramer as shown in Fig. 6B. In cytotoxicity assays, neither M17 nor M14 were susceptible to lysis by activated NK cells (Fig. 7A), whereas A375 and DM6 were killed in a dose-dependent manner at the indicated E/T ratios. Expression of MICA and MICB rendered M14 cells sensitive to murine NK lysis as shown at multiple E/T ratios (Fig. 7B) compared with control M14 cells. In multiple independent experiments (n = 6), the expression of either MICA or MICB was sufficient to render M14 melanoma sensitive to NOD-*scid* NK cell lysis (Fig. 7C). The involvement of muNKG2D receptor in melanoma recognition was examined using the antagonistic anti-muNKG2D mAb C7 (28). Pretreatment of activated NK

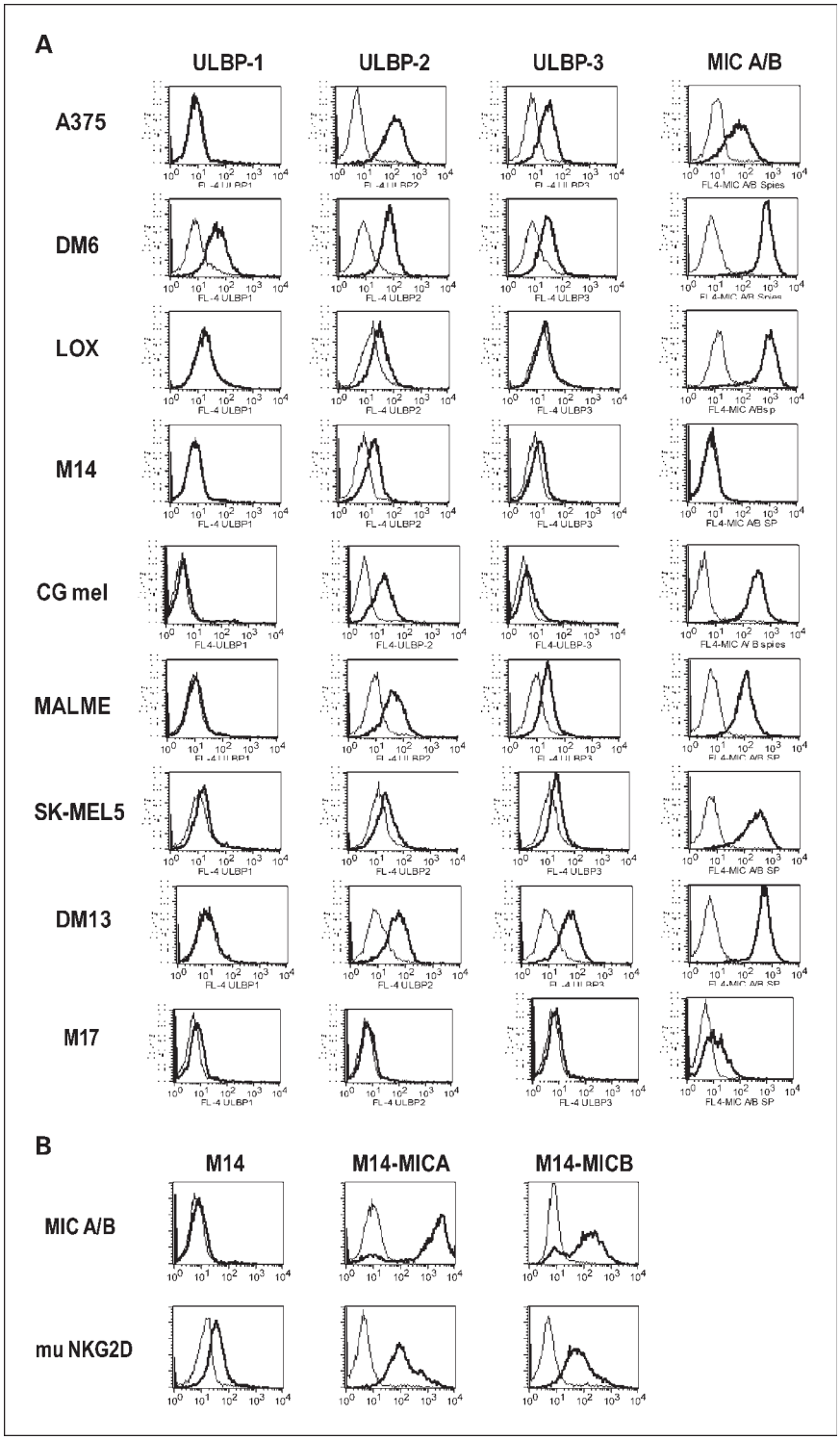

Fig. 6. Expression of NKG2D ligands, MICA/B, and ULBP 1 to 3, by human melanoma cell lines. *A,* melanoma cell lines were stained using anti-ULBPs and the 6D4 anti-MICA/B mAbs and analyzed by flow cytometry. ULBPs and MICA/B expression (*thick line*) and the isotype control (*thin line*) are shown in each histogram. Data are representative of three independent experiments. *B,* M14, M14-MICA, and M14-MICB cells were stained with anti-MICA/B 6D4 (*top*; *thick line*), isotype control (*top*; *thin line*), or muNKG2D tetramer (*bottom*; *thick line*), or control tetramer (*bottom*; *thin line*). Data are representative of two independent experiments.

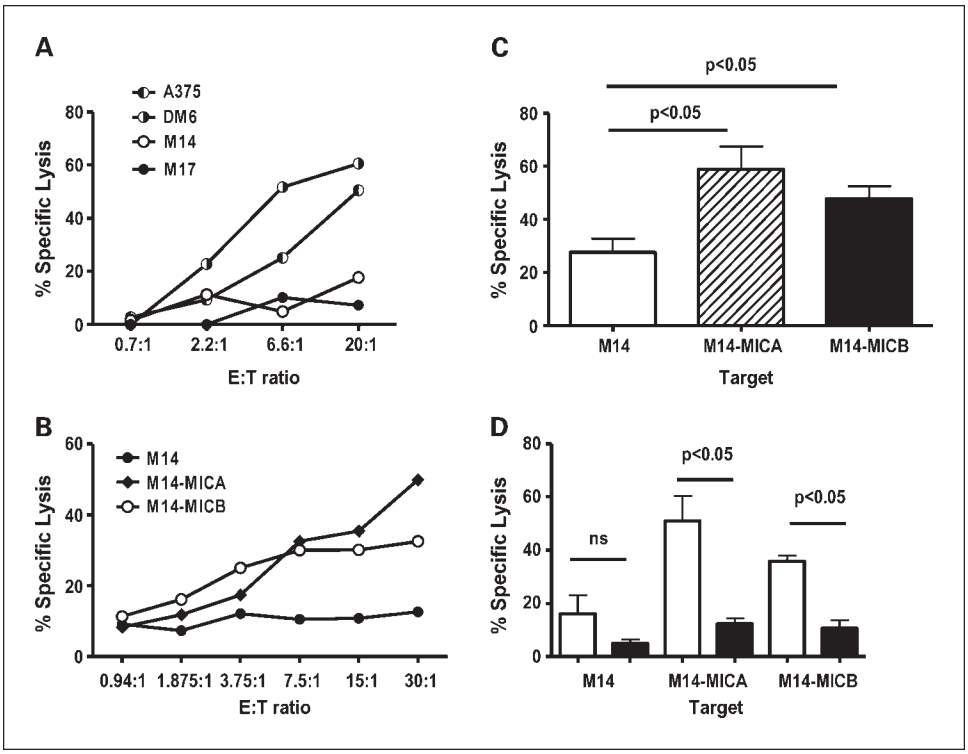

Fig. 7. Human melanoma recognition by NOD-*scid* NK cells correlates with MICA/B expression and is blocked by antimuNKG2D antibody. *A,* NOD-*scid* spleen cells were activated with IL-15 + IL-18 for 48 h, harvested, and incubated with ^{51}Cr-labeled targets for 4 h as described in Materials and Methods (n = 3 experiments). MICA/B expression by M14, M17, A375, and DM6 is shown in Fig. 6. *B,* NOD-*scid* NK cells were tested at the indicated E/T ratios in ^{51}Cr-release assay using M14, M14-MICA, and M14-MIB transfectants (n = 3 experiments). *C,* recognition of M14-MICA and M14-MICB transfectants by NK cells from NOD-*scid* mice. Columns, mean value at a 30:1 E/T ratio is shown from 6 independent experiments; bars, SD. The lower killing of M14-MICB (compared with MICA) likely reflects the lower antigen expression level on the M14-MICB target cell population. *D,* recognition of M14-MICA and M14-MICB by NOD-*scid* NK cells is blocked by antimuNKG2D mAb. NOD-*scid* spleen cells were cultured in IL-15 + IL-18 for 48 h, harvested, and incubated with anti-muNKG2D mAb (*black bars*) or isotype control (*white bars*) for 1 h (30 ug/mL), ^{51}Cr-labeled target cells added and assay done as described in Materials and Methods. E/T ratio is 30:1 (n = 3 experiments). Data in *C* and *D* was analyzed by repeated measure one-way ANOVA followed by Tukey's analysis. *P* values of <0.05 are statistically significant.

cells with anti-NKG2D mAb resulted in a significant decrease in MICA and MICB recognition with no statistically significant effect on control M14 cells (Fig. 7D). Altogether, these data support the finding that MICA and MICB are capable of binding to and activating murine NK cells through interaction with their NKG2D receptor.

Discussion

In the present study, we compared *scid*, NOD-*scid*, NOD-*scid*-$\beta 2m^{null}$, and NOD-*scid IL2R*γ^{null} mice as recipients for human melanoma. Engraftment of human melanoma pulmonary metastasis in NOD-*scid IL2R*γ^{null} mice is brisk and reproducible relative to the other strains examined. Despite multiple attempts to isolate and grow NK cells from NOD-*scid IL2R*γ^{null} mice, we were unsuccessful and, thus, confirm the original observation that ablation of the common cytokine-receptor γ-chain (*IL2R*γ) confers an absolute NK cell deficiency (13). Our results also suggest that murine NK cells use NKG2D to recognize MICA/B, and we propose that this mechanism accounts for the increased xenograft rejection observed in *scid*, NOD-*scid*, and NOD-*scid*-$\beta 2m^{null}$ mice.

We initially observed dramatic differences in human melanoma engraftment among NOD-*scid* $\beta 2m^{null}$ littermates and were perplexed by this inconsistency. Although NK cells from NOD-*scid* $\beta 2m^{null}$ mice are present in similar percentages as *scid* and NOD-*scid* animals, it seems that NK cells that develop in a MHC class I–deficient environment are functionally impaired (11, 36). However, our findings suggest the presence of residual/partial NK cell activity in NOD-*scid* $\beta 2m^{null}$ mice because some animals clearly have delayed tumor engraftment (Fig. 3B). The variable engraftment rates of human CD34+ stem cells in NOD-*scid* $\beta 2m^{null}$ animals supports this conclusion (37). In support of NK cells retarding the growth of xenografts, administration of anti-CD122 antibody to deplete endogenous NK cells in NOD-*scid* mice has been shown to improve engraftment of human hematopoietic stem cells (38) as well as solid tumor stem cells (39). The inconsistent tumor growth seen is likely to reflect variable levels of NK function among mouse strains and not heterogeneity in tumor sample as similar results were obtained using tumor lines or clones obtained by limiting dilution (data not shown). The inherent advantage of using the NOD-*scid IL2R*γ^{null} strain is that gene ablation of the IL2Rγ chain leads to absolute NK deficiency (12, 13) and results in remarkable consistency of human melanoma engraftment (this study). Additionally, NOD-*scid IL2R*γ^{null} do not develop thymic lymphoma with age, thus allowing for long-term studies in these mice. In contrast, NOD-*scid* and NOD-*scid* $\beta 2m^{null}$ animals have a high incidence of thymic lymphomas that are fatal (10).

NK function is regulated by inhibitory and activating cell surface receptors (40). NKG2D, a C-type lectin-like molecule, is a major NK activating receptor that interacts with a diverse array of ligands (41, 42). NKG2D ligands include retinoic acid early transcript 1 proteins and minor histocompatibility protein H60 and MULTI in mice and MICA, MICB, and ULBPs in human (32). Recent data in both NKG2D-deficient mice and gain-of-function studies using a novel chimeric NKG2D construct support the critical role of NKG2D in tumor surveillance (43, 44). Human melanomas and various carcinomas have been reported to express MICA/B and/or ULBPs and both ligands have been shown to be involved in human NK recognition of tumors (20, 45). Interestingly, NKG2D from one species can bind ligands from another; for example muNKG2D has been previously shown to bind human ligands MICB, ULBP-1, and ULBP-2 (33, 34). Several previous studies have examined NK cell function in NOD mice and shown some degree of impairment in target cell recognition (compared with the C57BL/6 strain; refs. 46, 47); however, little direct information regarding NOD-*scid* NK cell function in the context of xenograft recognition is available. Our results show that MICA/B-muNKG2D interaction leads to recognition of human melanoma, which may, in turn, result in decreased tumor engraftment in certain immunodeficient strains. The beige-scid mouse has also been reported to be permissive to human melanoma xenografts and as shown by Elsner and colleagues (48), MICA/B seems to be the tumor associated rejection ligand recognized by muNKG2D. Interestingly, beige-scid mice have large numbers of DX5+ NK cells that express low levels of NKG2D (data not shown). Thus, our results are consistent with the observation that murine NKG2D recognition of MICA/B and ULBPs may prevent/delay engraftment of many human solid tumors in immunodeficient mouse strains.

Small animal imaging provides significant advantages to monitor tumor growth in experimental models (49). Whole body BLI with luciferase reporters is remarkably sensitive, facile to execute, serially, and allows detection of early metastases in various tissues. MRI is less sensitive but has inherent advantages including superior spatial resolution and no requirement for reporter constructs. A recent report evaluating positron-emission tomography, X-ray computed tomography, and BLI modalities documents the ability for detecting human melanoma lung metastases (A375-M) in *scid* mice at day 45 (50). In our model, ^{18}F-FDG-PET imaging was done on several animals, which could, in fact, detect A375-RhoC lung metastases as early as day 30 (data not shown).

In summary, our study highlights muNKG2D recognition of MICA/B as an important receptor-ligand interaction used by NK cells in immunodeficient strains to limit engraftment of human tumors. Because NOD-*scid IL2R*γ^{null} mice have an absolute NK cell deficiency as well as additional innate and adaptive defects, this strain seems to be the best recipient for human melanoma.

Disclosure of Potential Conflicts of Interest

No potential conflicts of interest were disclosed.

Acknowledgments

We thank Richard Hynes, John DiPersio, Timothy Graubert, Marco Colonna, and Thomas Spies for reagents; Julie Ritchey and Matthew Holt for excellent technical assistance; Siteman Cancer Center High Speed Cell Sorter Core and Small Animal Cancer Imaging Core facilities for expert assistance; and Wayne Yokoyama and Todd Fehniger for advice.

References

1. Talmadge JE, Singh RK, Fidler IJ, Raz A. Murine models to evaluate novel and conventional therapeutic strategies for cancer. Am J Pathol 2007;170:793–804.
2. Guy-Grand D, Azogui O, Celli S, et al. Extrathymic T cell lymphopoiesis: ontogeny and contribution to gut intraepithelial lymphocytes in athymic and euthymic mice. J Exp Med 2003;197:333–41.
3. Biron CA, Young HA, Kasaian MT. Interleukin 2-induced proliferation of murine natural killer cells *in vivo*. J Exp Med 1990;171:173–88.
4. Mattern J, Bak M, Hahn EW, Volm M. Human tumor xenografts as model for drug testing. Cancer Metastasis Rev 1988;7:263–84.
5. Giovanella BC, Vardeman DM, Williams LJ, et al. Heterotransplantation of human breast carcinomas in nude mice. Correlation between successful heterotransplants, poor prognosis and amplification of the HER-2/neu oncogene. Int J Cancer 1991;47:66–71.
6. Bubenik J, Kieler J, Jandlova T, Simova J. Age-related decrease in transplantability of human tumours in nu/nu mice. Anticancer Res 1992;12:1695–8.
7. Marangoni E, Vincent-Salomon A, Auger N, et al. A new model of patient tumor-derived breast cancer xenografts for preclinical assays. Clin Cancer Res 2007;13:3989–98.
8. Greiner DL, Hesselton RA, Shultz LD. SCID mouse models of human stem cell engraftment. Stem Cells 1998;16:166–77.
9. Hudson WA, Li Q, Le C, Kersey JH. Xenotransplantation of human lymphoid malignancies is optimized in mice with multiple immunologic defects. Leukemia 1998;12:2029–33.
10. Shultz LD, Ishikawa F, Greiner DL. Humanized mice in translational biomedical research. Nat Rev Immunol 2007;7:118–30.
11. Kim S, Poursine-Laurent J, Truscott SM, et al. Licensing of natural killer cells by host major histocompatibility complex class I molecules. Nature 2005;436:709–13.
12. Shultz LD, Lyons BL, Burzenski LM, et al. Human lymphoid and myeloid cell development in NOD/LtSz-scid IL2R γ null mice engrafted with mobilized human hemopoietic stem cells. J Immunol 2005;174:6477–89.
13. Cao X, Shores EW, Hu-Li J, et al. Defective lymphoid development in mice lacking expression of the common cytokine receptor γ chain. Immunity 1995;2:223–38.
14. Ito M, Hiramatsu H, Kobayashi K, et al. NOD/SCID/γc^{null} mouse: an excellent recipient mouse model for engraftment of human cells. Blood 2002;100:3175–82.
15. Clark EA, Golub TR, Lander ES, Hynes RO. Genomic analysis of metastasis reveals an essential role for RhoC. Nature 2000;406:532–5.
16. Hakem A, Sanchez-Sweatman O, You-Ten A, et al. RhoC is dispensable for embryogenesis and tumor initiation but essential for metastasis. Genes Dev 2005;19:1974–79.
17. Collisson EA, De A, Suzuki H, Gambhir SS, Kolodney MS. Treatment of metastatic melanoma with an orally available inhibitor of the Ras-Raf-MAPK cascade. Cancer Res 2003;63:5669–73.
18. Craft N, Bruhn KW, Nguyen BD, et al. Bioluminescent imaging of melanoma in live mice. J Invest Dermatol 2005;125:159–65.
19. Darrow TL, Slingluff CL, Jr., Seigler HF. The role of HLA class I antigens in recognition of melanoma cells by tumor-specific cytotoxic T lymphocytes. Evidence for shared tumor antigens. J Immunol 1989;142:3329–35.
20. Pende D, Rivera P, Marcenaro S, et al. Major histocompatibility complex class I-related chain A and UL16-binding protein expression on tumor cell lines of different histotypes: analysis of tumor susceptibility to NKG2D-dependent natural killer cell cytotoxicity. Cancer Res 2002;62:6178–86.
21. Groh V, Bahram S, Bauer S, Herman A, Beauchamp M, Spies T. Cell stress-regulated human major histocompatibility complex class I gene expressed in gastrointestinal epithelium. Proc Natl Acad Sci U S A 1996;93:12445–50.
22. Groh V, Steinle A, Bauer S, Spies T. Recognition of stress-induced MHC molecules by intestinal epithelial γδ T cells. Science 1998;279:1737–40.
23. Welte SA, Sinzger C, Lutz SZ, et al. Selective intracellular retention of virally induced NKG2D ligands by the human cytomegalovirus UL16 glycoprotein. Eur J Immunol 2003;33:194–203.
24. Gross S, Piwnica-Worms D. Monitoring proteasome activity in cellulo and in living animals by bioluminescent imaging: technical considerations for design and use of genetically encoded reporters. Methods Enzymol 2005;399:512–30.
25. Garbow JR, Zhang Z, You M. Detection of primary lung tumors in rodents by magnetic resonance imaging. Cancer Res 2004;64:2740–2.
26. Garbow JR, Wang M, Wang Y, Lubet RA, You M. Quantitative monitoring of adenocarcinoma

development in rodents by magnetic resonance imaging. Clin Cancer Res 2008;14:1363–7.

27. Garbow J, Dugas J, Song S-K, Conradi M. A simple, robust hardware device for passive or active respiratory gating in MRI and MRS experiments. Concepts in magnetic resonance, Part B: Magnetic resonance engineering 2004;21B:40–8.

28. Ho EL, Carayannopoulos LN, Poursine-Laurent J, et al. Costimulation of multiple NK cell activation receptors by NKG2D. J Immunol 2002;169: 3667–75.

29. Carayannopoulos LN, Naidenko OV, Fremont DH, Yokoyama WM. Cutting edge: murine UL16-binding protein-like transcript 1: a newly described transcript encoding a high-affinity ligand for murine NKG2D. J Immunol 2002;169: 4079–83.

30. Carter L, Fouser LA, Jussif J, et al. PD-1:PD-L inhibitory pathway affects both CD4(+) and CD8 (+) T cells and is overcome by IL-2. Eur J Immunol 2002;32:634–43.

31. Gross S, Piwnica-Worms D. Spying on cancer: molecular imaging *in vivo* with genetically encoded reporters. Cancer Cell 2005;7:5–15.

32. Eagle RA, Trowsdale J. Promiscuity and the single receptor: NKG2D. Nat Rev Immunol 2007;7:737–44.

33. Diefenbach A, Jamieson AM, Liu SD, Shastri N, Raulet DH. Ligands for the murine NKG2D receptor: expression by tumor cells and activation of NK cells and macrophages. Nat Immunol 2000; 1:119–26.

34. Sutherland CL, Rabinovich B, Chalupny NJ, Brawand P, Miller R, Cosman D. ULBPs, human ligands of the NKG2D receptor, stimulate tumor immunity with enhancement by IL-15. Blood 2006;108:1313–9.

35. Pawelec G, Marsh SG. ESTDAB: a collection of immunologically characterised melanoma cell lines and searchable databank. Cancer Immunol Immunother 2005;55:623–7.

36. Dorfman JR, Zerrahn J, Coles MC, Raulet DH. The basis for self-tolerance of natural killer cells in β2-microglobulin- and TAP-1- mice. J Immunol 1997;159:5219–25.

37. Kollet O, Peled A, Byk T, et al. β2 microglobulin-deficient (β2mnull) NOD/SCID mice are excellent recipients for studying human stem cell function. Blood 2000;95:3102–5.

38. Shultz LD, Banuelos SJ, Leif J, et al. Regulation of human short-term repopulating cell (STRC) engraftment in NOD/SCID mice by host CD122+ cells. Exp Hematol 2003;31:551–8.

39. O'Brien CA, Pollett A, Gallinger S, Dick JE. A human colon cancer cell capable of initiating tumour growth in immunodeficient mice. Nature 2007;445:106–10.

40. Caligiuri MA. Human natural killer cells. Blood 2008;112:461–9.

41. Gonzalez S, Groh V, Spies T. Immunobiology of human NKG2D and its ligands. Curr Top Microbiol Immunol 2006;298:121–38.

42. Raulet DH. Roles of the NKG2D immunoreceptor and its ligands. Nat Rev Immunol 2003;3:781–90.

43. Guerra N, Tan YX, Joncker NT, et al. NKG2D-deficient mice are defective in tumor surveillance in models of spontaneous malignancy. Immunity 2008;28:571–80.

44. Zhang T, Barber A, Sentman CL. Generation of antitumor responses by genetic modification of primary human T cells with a chimeric NKG2D receptor. Cancer Res 2006;66:5927–33.

45. Pende D, Cantoni C, Rivera P, et al. Role of NKG2D in tumor cell lysis mediated by human NK cells: cooperation with natural cytotoxicity receptors and capability of recognizing tumors of nonepithelial origin. Eur J Immunol 2001;31: 1076–86.

46. Ogasawara K, Hamerman JA, Hsin H, Chikuma S, Bour-Jordan H, Chen, et al. Impairment of NK cell function by NKG2D modulation in NOD mice. Immunity 2003;18:41–51.

47. Johansson SE, Hall H, Bjorklund J, Hoglund P. Broadly impaired NK cell function in non-obese diabetic mice is partially restored by NK cell activation *in vivo* and by IL-12/IL-18 *in vitro.* Int Immunol 2004;16:1–11.

48. Muppala ElsnerL, Gehrman V, et al. The heat shcok protein HSP70 promotes mouse NK cell activity against tumors that express inducible NKG2CD ligands. J Immunol 2007;179:5523–33.

49. Contag CH. *In vivo* pathology: seeing with molecular specificity and cellular resolution in the living body. Annu Rev Pathol 2007;2:277–305.

50. Deroose CM, De A, Loening AM, et al. Multimodality imaging of tumor xenografts and metastases in mice with combined small-animal PET, small-animal CT, bioluminescence imaging. J Nucl Med 2007;48:295–303.

Clinical Cancer Research

Immunodeficient Mouse Strains Display Marked Variability in Growth of Human Melanoma Lung Metastases

Beatriz M. Carreno, Joel R. Garbow, Grant R. Kolar, et al.

Clin Cancer Res 2009;15:3277-3286.